Supporting Information

Efficient photocatalytic water oxidation catalyzed by polyoxometalate of $[Fe_{11}(H_2O)_{14}(OH)_2(W_3O_{10})_2(\alpha\text{-}SbW_9O_{33})_6]^{27-}$ based on abundant metals

Xiaoqiang Du[a], Yong Ding [ab*], Fangyuan Song [a], Baochun Ma[a], Junwei Zhao [c], Jie Song [d]

[a] *State Key Laboratory of Applied Organic Chemistry, Key Laboratory of Nonferrous Metals Chemistry and Resources Utilization of Gansu Province, and College of Chemistry and Chemical Engineering, Lanzhou University, Lanzhou 730000, China*

[b] *State Key Laboratory for Oxo Synthesis and Selective Oxidation, Lanzhou Institute of Chemical Physics, Chinese Academy of Sciences, Lanzhou 730000, China*

[c] *Henan Key Laboratory of Polyoxometalate Chemistry, College of Chemistry and Chemical Engineering, Henan University, Kaifeng, Henan 475004 (P.R. China)*

[d] *Department of Biomedical Engineering, Emory University and Georgia Institute of Technology, Atlanta, Georgia 30322, USA*

* To whom correspondence should be addressed.
E-mail addresses: dingyong1@lzu.edu.cn

Quantum Yield Calculation

Initial O_2 formation rate = 0.13 μmol·s^{-1}

Irradiation radius = 1 cm = 0.01 m

Photon flux = $\pi \times (0.01\text{m})^2 \times 1748$ μmol·m^{-2}·s^{-1} = 0.549 μmol·s^{-1}

$$\Phi_{QY(initial)} = 2 \times \frac{\text{initial } O_2 \text{ formation rate}}{\text{photon flux}} \times 100\%$$

$$= \frac{2 \times 0.13\ \mu\text{mol} \cdot \text{s}^{-1}}{0.549\ \mu\text{mol} \cdot \text{s}^{-1}} \times 100\%$$

$$= 47\%$$

Electrochemistry

H_2SO_4, Na_2SO_4, NaOH, H_3BO_3, $Na_2B_4O_7$ were commercial products. The pH = 3 medium was made up with 0.2 M Na_2SO_4 + H_2SO_4. The solutions were deaereated thoroughly for a least 30 min with pure argon and kept under a positive pressure of this gas during the experiments.

Equipment and Apparatus

Cyclic voltammetry (CV) was recorded on a CHI660D electrochemical analyzer, where a glassy carbon, an Ag/AgCl and a Pt wire electrodes were used as a working, reference and auxiliary electrodes, respectively. CV was obtained in buffer solutions containing 0.2 M $NaNO_3$ as a supporting electrolyte at room temperature with a scanning rate of 25 mV s^{-1}. UV-vis absorption spectra were recorded on Beijing Purkinje General Instrument Co.,Ltd. TU-1810 spectrophotometer equipped with a photomutiplier tube detector. Infrared spectra (2–4% (w/w) sample in KBr pellets) were performed using a Bruker VERTEX 70v FT-IR spectrometer. Elemental analysis of the catalysts was performed on TJA ICP-atomic emission spectrometer (IRIS Advantage ER/S). X-ray photoelectron spectra (XPS) were measured by ESCALAB250xi with X-Ray monochromatisation. GC-MS spectral analyses of isotopic labelled O_2 were performed on an Agilent Series 7890A model chromatograph interfaced with an Agilent Series 5975C model mass spectrometer. The capillary electrophoretic were performed on Beckman, MDQ. equipped with a 32.karat 7.0 software. Transmission electron microscope (TEM) images were obtained with a JEOL JEM-2010 instrument operated at 200 kV.

Isotope-Labeled Experiment

The 10.8 atom % $H_2{}^{18}O$ of borate buffer solution (pH 10.0, 80 mM) containing **1** (1.3 μM), $[Ru(bpy)_3](ClO_4)_2$ (1 mM), $Na_2S_2O_8$ (5 mM) was deaerated with Helium gas before irradiation by LED light ($\lambda \geq 420$ nm) in a flask that is sealed with a rubber septum. After 9 min, 50 μL of gas sample was withdrawn using a gas-tight syringe for gas analysis. An Agilent Series 7890A model chromatograph interfaced with an Agilent Series 5975C model mass spectrometer operating in electron impact ionization mode was used to collect mass spectrometric data. The MS detector was tuned for maximum sensitivity (quadrupole temperature, 150 ^oC; Ion source temperature, 230 ^oC). Single ion mode was used to scan for the ions m/z = 28, 32, 34, 36 with a dwell time of 100 ms, resulting in 8.3 cycles per second. The ions of m/z range from 30 to 50 were also scanned in order to observe the abundance change of $^{16}O^{18}O$ and $^{18}O^{18}O$, which evolved from $H_2{}^{16}O$ and $H_2{}^{18}O$, respectively. The total flow rate into the spectrometer was limited to 0.6 mL/min. The GC equipped with a molecular sieve column (30 m × 0.32 mm × 15 um), and the vaporizing chamber temperature and column temperature was set for 100 ^oC and 35 ^oC, respectively.

The preparing of $Na_{27}[Fe_{11}(H_2O)_{14}(OH)_2(W_3O_{10})_2(\alpha\text{-}SbW_9O_{33})_6]\cdot 103H_2O$(1), $\alpha\text{-}Fe_2O_3$ nanoparticles, $Na_6[Fe_4(H_2O)_{10}(SbW_9O_{33})_2]\cdot 40H_2O$ and $K_5SiFe(OH)_2W_{11}O_{39}\cdot 14H_2O$

$Na_{27}[Fe_{11}(H_2O)_{14}(OH)_2(W_3O_{10})_2(\alpha\text{-}SbW_9O_{33})_6]\cdot 103H_2O$ were prepared according to a published method[1] and all the characterizations of **1** were reported in published literature[1]. $\alpha\text{-}Fe_2O_3$ nanoparticles with size of 60 nm, (Figure S13) were prepared according to a published method[2]. $Na_6[Fe_4(H_2O)_{10}(SbW_9O_{33})_2]\cdot 40H_2O$ were prepared according to a published method[3] and $K_5SiFe(OH)_2W_{11}O_{39}\cdot 14H_2O$ were prepared according to a published method.[4]

The measurement of Quantum Yield

The quantum yields of O_2 evolution were determined for the photocatalytic water oxidation under the following conditions. A quartz flask containing a borate buffer solution (80 mM, pH 10.0, 16 mL) with **1** (1.3 μM), $[Ru(bpy)_3](ClO_4)_2$ (1 mM) and $Na_2S_2O_8$ (5 mM) was irradiated by an interference filtered (Asahi spectra SV 490) from a LED source ($420 < \lambda < 490$ nm) described above. The photon flux of the incident light was determined using a Ray virtual radiation

actinometer (FU 100, silicon ray detector, light spectrum, 400-700 nm; sensitivity, 10-50 μV $\mu mol^{-1}\ m^{-2}\ s^{-1}$), affording a value to be 1748 μmol $m^{-2}\ s^{-1}$.

Laser flash photolysis

Nanosecond transient absorption measurements were performed on an Edinburgh Instruments LP920-KS laser flash photolysis spectrometer, using an OPO laser source (OPOTEK Vibrant). Transient detection was obtained using a photomultiplier-oscilloscope combination (Hamamatsu R928P, Tektronix TDS3012C). Kinetics of bleach recovery conditions: Excitation wavelength = 445 nm, analysis wavelength = 450 nm; 50 μM $[Ru(bpy)_3]^{2+}$; 5 mM $Na_2S_2O_8$; 0-100 μM **1**; pH 10.0, 80 mM borate buffer.

Photocatalytic Water Oxidation

Photocatalytic water oxidation was performed as follows. The desired concentration of catalyst (0.33–2.60 μM) was added to a buffer solution (80 mM, pH 8.0–11.0 for borate buffer) containing $[Ru(bpy)_3](ClO_4)_2$ (1.0 mM) and $Na_2S_2O_8$ (5.0 mM). The above solution was deaerated by purging with Ar gas for 5 min in a flask (21 mL) sealed with a rubber septum (the volume of reaction solution was 16 mL). The reaction was then started by irradiating the solution with a LED light source (light intensity 16 mW, beam diameter 2 cm) through a transmitting glass filter ($\lambda \geq 420$ nm) at room temperature. After each irradiation time, 150 μL of Ar was injected into the flask and then the same volume of gas in the headspace of the flask was withdrawn by a SGE gas-tight syringe and analysed by gas chromatography (GC). The O_2 in the sampled gas was separated by passing through a 2 m × 3 mm packed molecular sieve 5A column with an Ar carrier gas and quantified by a thermal conductivity detector (TCD) (Shimadzu GC-9A). The total amount of evolved O_2 was calculated from the concentration of O_2 in the headspace gas. Contamination of the head-space with air was corrected by measuring of N_2 present in the head-space (from the N_2 peak in the GC traces). The solution pH was measured after the reaction by a METTLER TOLEDO FEP20 pH meter.

Table S1. The BVS Values of Fe and Selected the Oxygen Atoms in 1

Atoms	BVS values	Atoms	BVS values	Atoms	BVS values
Fe1	3.23	Fe2	3.16	Fe3	3.20
Fe4	2.93	Fe5	3.00	Fe6	2.98
O1W	0.42	O3W	0.41	O109	1.99
O2W	0.34	O4W	0.42	O110	1.99
O5W	0.45	O6W	0.38	O7W	0.34

Table S2. Crystal Data and Structure Refinements for $Na_6[Fe_4(H_2O)_{10}(SbW_9O_{33})_2]\cdot 40H_2O$

Identification code	$Na_6[Fe_4(H_2O)_{10}(SbW_9O_{33})_2]\cdot 40H_2O$
Empirical formula	$H_{100}Fe_4Na_6O_{116}Sb_2W_{18}$
Formula weight	5752
Temperature/K	293(2)
Crystal system	monoclinic
Space group	$P2_1/c$
a/Å	16.1262(8)
b/Å	15.2572(5)
c/Å	20.2165(13)
α/°	90.00
β/°	96.061(7)
γ/°	90.00
Volume/Å^3	4946.3(4)
Z	2
ρ_{calc}mg/mm^3	3.908
m/mm^{-1}	47.815
F(000)	5164.0
Radiation	Cu Kα (λ = 1.54184)
2Θ range for data collection	8 to 145.32°
Index ranges	$-19 \le h \le 19$, $-18 \le k \le 18$, $-21 \le l \le 25$
Reflections collected	33341
Independent reflections	9794 [R_{int} = 0.0370]
Data/restraints/parameters	9794/12/658
Goodness-of-fit on F^2	1.042
Final R indexes [I≥2σ (I)]	R_1 [a] = 0.0250, wR_2 [b] = 0.0534
Final R indexes [all data]	R_1 [a] = 0.0320, wR_2 [b] = 0.0562
Largest diff. peak/hole / eÅ^{-3}	1.85/-1.15

[a] $R_1 = \Sigma||F_0| - |F_c|| / \Sigma|F_0|$; [b] $wR_2 = \Sigma[w(F_0^2 - F_c^2)^2]/\Sigma[w(F_0^2)^2]^{1/2}$

Table S3. Water Oxidation Catalyzed without 1 or $Ru(bpy)_3Cl_2$ or Persulfate

Entry	$[Ru(bpy)_3]Cl_2$ (mM)	$Na_2S_2O_8$ (mM)	Catalyst (μM)	O_2 (μmol)
1	1	5	0	1.9
2	1	0	1.3	0
3	0	5	1.3	0

Conditions: LED lamp ($\lambda \geq 420$ nm), 80 mM sodium borate buffer (initial pH 10.0), total reaction volume is 16 mL and overall volume is ~21 mL, vigorous agitation using a magnetic stirrer.

Table S4. Water Oxidation Catalyzed without 1 or $Ru(bpy)_3(ClO_4)_2$ or Persulfate

Entry	$[Ru(bpy)_3](ClO_4)_2$ (mM)	$Na_2S_2O_8$ (mM)	Catalyst (μM)	O_2 (μmol)
1	1	5	0	3.9
2	1	0	1.3	0
3	0	5	1.3	0

Conditions: LED lamp ($\lambda \geq 420$ nm), 80 mM sodium borate buffer (initial pH 10.0), total reaction volume is 16 mL and overall volume is ~21 mL, vigorous agitation using a magnetic stirrer.

Table S5. Water Oxidation Catalyzed without 1 under Different pH

Entry	pH (80 mM NaBi)	O_2 (μmol)
1	8.0	0.2
2	9.0	3.1
3	10.0	3.9
4	11.0	4.3

Conditions: LED lamp (λ ≥ 420 nm), 0 μM **1**, 1.0 mM $[Ru(bpy)_3](ClO_4)_2$, 5.0 mM $Na_2S_2O_8$, total reaction volume is 16 mL and overall volume is ~21mL, vigorous agitation using a magnetic stirrer.

Table S6. Water Oxidation Catalyzed by Fe_{11} POM under Different pH [a]

Entry	pH	O_2 (μmol)	O_2 yield(%)	TON	TOF(s^{-1})	$[Ru(bpy)_3](ClO_4)_2$ Degradation Percentage (%)
1[b]	5.8	0	0	0	0	Not studied
2[c]	8	3.4	8.6	164	0.9	51.5
3[c]	9	15.9	40	762	4.0	13.9
4[c]	10	37.8	94	1815	6.3	3.4
5[c]	11	26.8	67	1290	5.0	6.3

[a] Conditions: LED lamp (λ ≥ 420 nm), 1.3 μM Fe_{11} POM, 1.0 mM $[Ru(bpy)_3](ClO_4)_2$, 5.0 mM $Na_2S_2O_8$, total reaction volume is 16 mL and overall volume is ~21mL, vigorous agitation using a magnetic stirrer. Dye degradation was evaluated by using UV-vis spectrosocpy (Figure S 18 -23).

[b] 20 mM Na_2SiF_6 buffer

[c] 80mM borate buffer,

Table S7. TON, $TOF_{initial}$ and Quantum Yield of Photocatalytic Water Oxidation Catalyzed by Different Catalysts

Catalyst	Representative reaction conditions	TON	TOF	$\Phi_{QY(initial)}$ %	Ref.
1	LED lamp ($\lambda \geq 420$ nm), 1.3 μM catalyst, 1.0 mM $[Ru(bpy)_3](ClO_4)_2$, 5.0 mM $Na_2S_2O_8$, 80 mM sodium borate buffer (pH 10.0)	1815	6.3 s^{-1}	47	This work
$Na_{10}[Co_4(H_2O)_2(\alpha\text{-}PW_9O_{34})_2]$	Xe lamp (420–470 nm), 5 μM catalyst, 1.0 mM $[Ru(bpy)_3]Cl_2$, 5.0 mM $Na_2S_2O_8$, 80 mM sodium borate buffer (pH 8.0)	224	No data	30	5
$K_{10.2}Na_{0.8}[\{Co_4(\mu\text{-}OH)(H_2O)_3\}(Si_2W_{19}O_{70})]$	Xe lamp (420–520 nm), 10 μM catalyst, 1.0 mM $[Ru(bpy)_3]Cl_2$, 5 mM $Na_2S_2O_8$, 25 mM sodium borate buffer (pH 9.0)	80	0.1 s^{-1}	No data	6
$(NH_4)_3[CoMo_6O_{24}H_6]$	300 W Xe lamp (400–800 nm), 0.4 mM $[Ru(bpy)_3](NO_3)_2$, 3 mM $Na_2S_2O_8$, 0.1 M borate buffer solution (pH 8.0)	107 (Based on 3.6 μM catalyst)	0.11 s^{-1} (Based on 20 μM catalyst)	54	7
$(NH_4)_6[Co_2Mo_{10}O_{38}H_4]$	300 W Xe lamp (400–800 nm), 0.4 mM $[Ru(bpy)_3](NO_3)_2$, 3 mM $Na_2S_2O_8$, 0.1 M borate buffer solution (pH 8.0)	154 (Based on 1.9 μM catalyst)	0.16 s^{-1} (Based on 10 μM catalyst)	42	7
Trans-$[Co^{II}(qpy)(OH_2)_2](ClO_4)_2$	500 W mercury arc lamp (457 nm), 0.2 μM catalyst, 128 μM $[Ru(bpy)_3]Cl_2$, 5 mM $Na_2S_2O_8$, 15 mM borate buffer solution (pH 8.0)	355 (Reaction time = 1.5 h)	No data	No data	8
$[Co^{II}(Me_6tren)(OH_2)](ClO_4)_2$	500 W Xe lamp ($\lambda > 420$ nm), 5.0 μM catalyst, 0.5 mM $[Ru(bpy)_3](ClO_4)_2$, 10 mM $Na_2S_2O_8$, 100 mM borate buffer solution (pH 9.0)	420 (Decomposed to $Co(OH)_x$)	No data	32	9
$[Co^{III}(Cp^*)(bpy)(OH_2)](PF_6)_2$	500 W Xe lamp ($\lambda > 420$ nm), 5.0 μM catalyst, 0.5 mM $[Ru(bpy)_3](ClO_4)_2$, 10 mM $Na_2S_2O_8$, 100 mM borate buffer solution (pH 9.0)	320 (Decomposed to $Co(OH)_x$)	No data	30	9
$Co^{III}_4O_4(OAc)_4(py)_4$	250W high power Arc lamp (450 nm), 41.5 μM catalyst, 0.5 mM $[Ru(bpy)_3]Cl_2$, 10.5 mM $Na_2S_2O_8$, HCO_3^- buffer (pH 7.0)	40	0.02 s^{-1}	No data	10

$K_{10}H_2[Ni_5(OH)_6(OH_2)_3(Si_2W_{18}O_{66})_2]$	17 mW LED light (455 nm), 1.0 mM $[Ru(bpy)_3]Cl_2$, 5.0 mM $Na_2S_2O_8$, 80 mM sodium borate buffer (pH 8.0)	60 (Based on 2μM catalyst)	1 s^{-1}(the first 10 Seconds)	3.8	[11]
$Cs_9[(\gamma\text{-}PW_{10}O_{36})_2Ru_4O_5(OH)(H_2O)_4$	Xe lamp (420–520 nm), 5.1μM catalyst, 1.0 mM $[Ru(bpy)_3]Cl_2$, 5 mM $Na_2S_2O_8$,20 mM Na_2SiF_6 buffer (pH 5.8)	120	0.13 s^{-1}	No data	[12]
α-$K_6Na[\{Ru_3O_3(H_2O)Cl_2\}(SiW_9O_{34})$	LED lamp (470 nm), 50μM catalyst, 1 mM $[Ru(bpy)_3]Cl_2$, 5 mM $Na_2S_2O_8$, 20 mM Na_2SiF_6 buffer (pH 5.8)	23	0.7 s^{-1}	No data	[13]
α-$K_{11}Na_1[Co_4(H_2O)_2(SiW_9O_{34})_2]$	LED lamp(470 nm) 1 mM $[Ru(bpy)_3]Cl_2$, 5 mM $Na_2S_2O_8$, 20 mM Na_2SiF_6 buffer (pH 5.8)	24 (Based on 20μM catalyst)	0.4 s^{-1} (Based on 42μM catalyst)	No data	[13]
$Ru^{II}(hqc)(pic)_3$	A 500 W xenon lamp (λ > 400 nm), 55.0 μM catalyst, 550 μM $[Ru\text{-}(bpy)_3]^{2+}$, 10mM $S_2O_8^{2-}$, 20 mM phosphate buffer (pH 7.2)	< 5	No data	No data	[14]
	A 500 W xenon lamp (λ > 400 nm), 55.0 μM catalyst, 550 μM $[Ru\text{-}(bpy)_2(dcbpy)]^{2+}$, 10 mM $S_2O_8^{2-}$, 20 mM phosphate buffer (pH 7.2)	42	No data	No data	[14]
	A 500 W xenon lamp (λ > 400 nm), 55.0 μM catalyst, 550 μM $[Ru\text{-}(bpy)(dcbpy)_2]^{2+}$, 10mM $S_2O_8^{2-}$, 20 mM phosphate buffer (pH 7.2)	61	No data	9	[14]
$Fe(mcp)Cl_2$	A 200 W Xe lamp (λ > 420 nm), 1.0 mM Catalyst, 0.2 mM $[Ru(bpy)_3]Cl_2$, 2mM $Na_2S_2O_8$, 15 mM borate buffer (pH 8.5) at 23 °C	194	No data	No data	[15]
$[Fe(bpy)_2Cl_2]Cl$	A 200 W Xe lamp (λ > 420 nm), 1.0 mM Catalyst, 0.2 mM $[Ru(bpy)_3]Cl_2$, 2mM $Na_2S_2O_8$, 15 mM borate buffer (pH 8.5) at 23 °C	157	No data	No data	[15]
$[Fe(tpy)_2]Cl_2$	A 200 W Xe lamp (λ > 420 nm), 1.0 mM Catalyst, 0.2 mM $[Ru(bpy)_3]Cl_2$, 2mM $Na_2S_2O_8$, 15 mM borate buffer (pH 8.5) at 23 °C	376	No data	No data	[15]
$[Fe(cyclen)Cl_2]C$	A 200 W Xe lamp (λ > 420 nm), 1.0 mM	412	No data	No data	[15]

1	Catalyst, 0.2 mM $[Ru(bpy)_3]Cl_2$, 2mM $Na_2S_2O_8$, 15 mM borate buffer (pH 8.5) at 23 ^oC				
$Fe(tmc)Br_2$	A 200 W Xe lamp ($\lambda > 420$ nm), 1.0 mM Catalyst, 0.2 mM $[Ru(bpy)_3]Cl_2$, 2mM $Na_2S_2O_8$, 15 mM borate buffer (pH 8.5) at 23 ^oC	364	No data	No data	[15]
$Fe(ClO_4)_3$	A 200 W Xe lamp ($\lambda > 420$ nm), 1.0 mM Catalyst, 0.2 mM $[Ru(bpy)_3]Cl_2$, 2mM $Na_2S_2O_8$, 15 mM borate buffer (pH 8.5) at 23 ^oC	436	No data	No data	[15]
$Fe(BQEN)(OTf)_2$	A 500 W xenon lamp ($\lambda > 400$ nm), 5.0 μM catalyst, 0.25 mM $[Ru(bpy)_3]SO_4$, 5.0 mM $Na_2S_2O_8$, 100 mM sodium borate buffer (pH 9.0)	259	No data	No data	[16]
$Fe(BQCN)(OTf)_2$	A 500 W xenon lamp ($\lambda > 400$ nm), 5.0 μM catalyst, 0.25 mM $[Ru(bpy)_3]SO_4$, 5.0 mM $Na_2S_2O_8$, 100 mM sodium borate buffer (pH 9.0)	No data	No data	No data	[16]
$[Co^{II}_4(hmp)_4(\mu\text{-}OAc)_2(\mu_2\text{-}OAc)_2(H_2O)_2]$	LED lamp ($\lambda = 470$ nm), 60 μM catalyst, 1 mM $[Ru(bpy)_3]^{2+}$, 5 mM $Na_2S_2O_8$, , 50 mM borate (pH 9.0)	28	7 s^{-1}	No data	[17]
$[\{Co(H_2O)_3\}_2\{CoBi_2W_{19}O_{66}(OH)_4\}]^{10-}$	LED lamp (470 nm), 115 μM catalyst, 1 mM $[Ru(bpy)_3]Cl_2$, 5 mM $Na_2S_2O_8$, 20 mM Na_2SiF_6 buffer (pH 5.8)	21	No data	No data	[18]
$[NiL_3](ClO_4)_2$	500 W Xe lamp (λ=457 nm), 0.6 mM catalyst, 0.12 mM $[Ru(bpy)_3](ClO_4)_2$, 2.5 mM $Na_2S_2O_8$,30mM borate buffer (pH 8.0), T=23^oC	855	No data	No data	[19]
$[\{Co_4(OH)_3(PO_4)\}_4(SiW_9O_{34})_4]^{32-}$	A 300 W xenon lamp ($\lambda > 420$ nm), 20 μM catalyst, 1.0 mM $[Ru(bpy)_3]Cl_2$, 5.0 mM $Na_2S_2O_8$, 80 mM sodium borate buffer (pH 9.0)	22.5	0.053s^{-1}	No data	[20]
$[\{Co_4(OH)_3(PO_4)\}_4(GeW_9O_{34})_4]^{32-}$	A 300 W xenon lamp ($\lambda > 420$ nm), 20 μM catalyst, 1.0 mM $[Ru(bpy)_3]Cl_2$, 5.0 mM $Na_2S_2O_8$, 80 mM sodium borate buffer (pH 9.0)	38.75	0.105s^{-1}	No data	[20]

$[\{Co_4(OH)_3(PO_4)\}_4(PW_9O_{34})_4]^{28-}$	A 300 W xenon lamp (λ > 420 nm), 20 μM catalyst, 1.0 mM $[Ru(bpy)_3]Cl_2$, 5.0 mM $Na_2S_2O_8$, 80 mM sodium borate buffer (pH 9.0)	20.25	No data	No data	[20]
$[\{Co_4(OH)_3(PO_4)\}_4(AsW_9O_{34})_4]^{28-}$	A 300 W xenon lamp (λ > 420 nm), 20 μM catalyst, 1.0 mM $[Ru(bpy)_3]Cl_2$, 5.0 mM $Na_2S_2O_8$, 80 mM sodium borate buffer (pH 9.0)	33.0	No data	No data	[20]
$Na_{10}[Co_4(H_2O)_2(VW_9O_{34})_2]\cdot 35H_2O$	LED lamp (λ=455 nm), 0.2 μM catalyst, 1.0 mM $[Ru(bpy)_3]$ Cl_2, 5.0 mM $Na_2S_2O_8$, 80 mM sodium borate buffer (pH 9.0)	4210	$>1\times10^3 s^{-1}$	47.7	[21]
$K_{10}[Co\text{-}(H_2O)_2(\gamma\text{-}SiW_{10}O_{35})_2]\cdot 23H_2O$	LED lamp (λ ≥ 420 nm), 5.0 μM catalyst, 1.0 mM $[Ru(bpy)_3]$ Cl_2, 5.0 mM $Na_2S_2O_8$, 80 mM sodium borate buffer (pH 9.0)	186.9	$1.2 s^{-1}$	27	[22]
$Na_{24}[Ni_{12}(OH)_9(CO_3)_3(PO_4)(SiW_9O_{34})_3]\cdot 56H_2O$	A 300 W xenon lamp (λ > 420 nm), 2 μM catalyst, 1.0 mM $[Ru(bpy)_3]Cl_2$, 5.0 mM $Na_2S_2O_8$, 80 mM sodium borate buffer (pH 9.0)	85.6	$0.13 s^{-1}$	No data	[23]
$Na_{25}[Ni_{13}(H_2O)_3(OH)_9(PO_4)_4(SiW_9O_{34})_3]\cdot 50H_2O$	A 300 W xenon lamp (λ > 420 nm), 2 μM catalyst, 1.0 mM $[Ru(bpy)_3]Cl_2$, 5.0 mM $Na_2S_2O_8$, 80 mM sodium borate buffer (pH 9.0)	94.1	$0.15 s^{-1}$	No data	[23]
$Na_{50}[Ni_{25}(H_2O)_2(OH)_{18}(CO_3)_2(PO_4)_6(SiW_9O_{34})_6]\cdot 85H_2O$	A 300 W xenon lamp (λ > 420 nm), 2 μM catalyst, 1.0 mM $[Ru(bpy)_3]Cl_2$, 5.0 mM $Na_2S_2O_8$, 80 mM sodium borate buffer (pH 9.0)	124.4	$0.21 s^{-1}$	No data	[23]

$TOF_{initial}$ = $TON_{initial}$/60 s, $TON_{initial}$ = Molar of oxygen produced in 1 minute/Molar of **1**,

Φ_{QY}(quantum yield) = [(initial O_2 formation rate)/(photon flux)].

Table S8.TON and $TOF_{initial}$ of Chemical Water Oxidation Catalyzed by Different Catalysts Containing Iron

Catalyst	Representative reaction conditions	TON	TOF	Ref.
1	LED lamp ($\lambda \geq 420$ nm), 1.3μM catalyst, 1.0 mM $[Ru(bpy)_3](ClO_4)_2$, 5.0 mM $Na_2S_2O_8$, 80 mM sodium borate buffer (pH 10.0)	1815	6.3 s^{-1}	This work
Fe-TAML (X_1= X_2=Cl, R= F. Y= H_2O)	182 mM $(NH_4)_2Ce(NO_3)_6$, 0.980 mM catalyst in water	16	1.3 s^{-1}	[24]
$[Fe(OTf)_2(^{Me2}Pytacn)]$	125 mM $(NH_4)_2Ce(NO_3)_6$, 37.5 μM catalyst in water (pH 1)	70±5	No data	[25]
$[Fe(OTf)_2(^{Me2}Pytacn)]$	125 mM $(NH_4)_2Ce(NO_3)_6$, 12.5 μM catalyst in water (pH 1)	82±8	No data	[25]
$[Fe(OTf)_2(mcp)]$	125 mM $(NH_4)_2Ce(NO_3)_6$, 37.5 μM catalyst in water (pH 1)	360±20	No data	[25]
$[FeCl_2(mcp)]$	125 mM $(NH_4)_2Ce(NO_3)_6$, 37.5 μM catalyst in water (pH 1)	320±15	No data	[25]
$[(Fe(mcp))_2(\mu\text{-}O)(\mu\text{-}OH)](OTf)_2$	125 mM $(NH_4)_2Ce(NO_3)_6$, 6.25 μM catalyst in water (pH 1)	210±21	No data	[25]
$[Fe(OTf)_2(mcp)]$	125 mM $NaIO_4$, 37.5 μM catalyst in water (pH 2)	＞1050	No data	[25]
$[Fe(OTf)_2(bpbp)]$	125 mM $(NH_4)_2Ce(NO_3)_6$, 37.5 μM catalyst in water (pH 1)	63±7	No data	[25]
$[Fe(OTf)_2(mep)]$	125 mM $(NH_4)_2Ce(NO_3)_6$, 37.5 μM catalyst in water (pH 1)	145±5	No data	[25]
$[Fe(OTf)_2(tpa)]$	125 mM $(NH_4)_2Ce(NO_3)_6$, 37.5 μM catalyst in water (pH 1)	40±4	No data	[25]
$Fe(BQEN)(OTf)_2$	125 mM $(NH_4)_2Ce(NO_3)_6$, 12.5 μM catalyst in nonbuffered aqueous solution	80±10	No data	[16]
$Fe(BQCN)(OTf)_2$	125 mM $(NH_4)_2Ce(NO_3)_6$,12.5 μM catalyst in nonbuffered aqueous solution	20±5	No data	[16]

$TOF_{initial}$ = $TON_{initial}$/60 s, $TON_{initial}$ = Molar of oxygen produced in 1 minute/Molar of **1**.

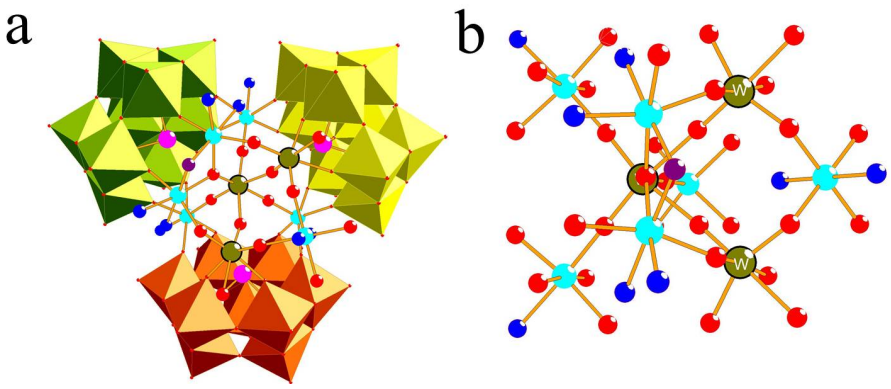

Figure S1. X-ray crystal structure of half-unit of **1a** in combined polyhedral and ball-and-stick representations. Color scheme: $[\alpha\text{-}SbW_9O_{33}]^{9-}$ polyhedra (lime, yellow, orange), Fe (cyan), O (red), H_2O (blue), OH (violet), Sb (pink), W (green).

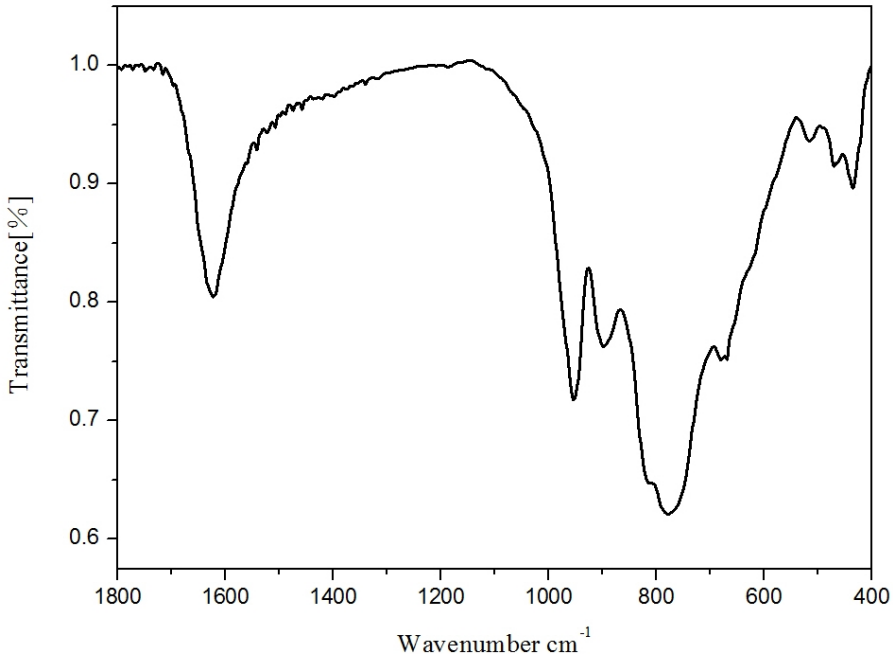

Figure S2. FT-IR spectrum of $Na_6[Fe_4(H_2O)_{10}(SbW_9O_{33})_2]\cdot 40H_2O$.

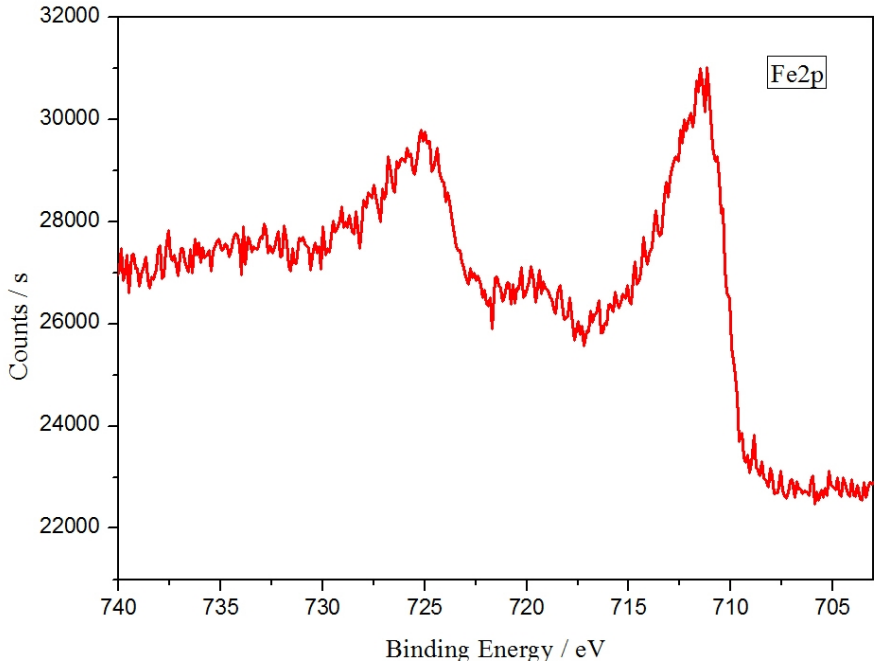

Figure S3. X-ray photoelectron spectra of **1** showing the region of Fe $2p_{3/2}$ and Fe $2p_{1/2}$ peaks of **1**. The binding energy of each element was normalized to the C 1s peak (284.8 eV).

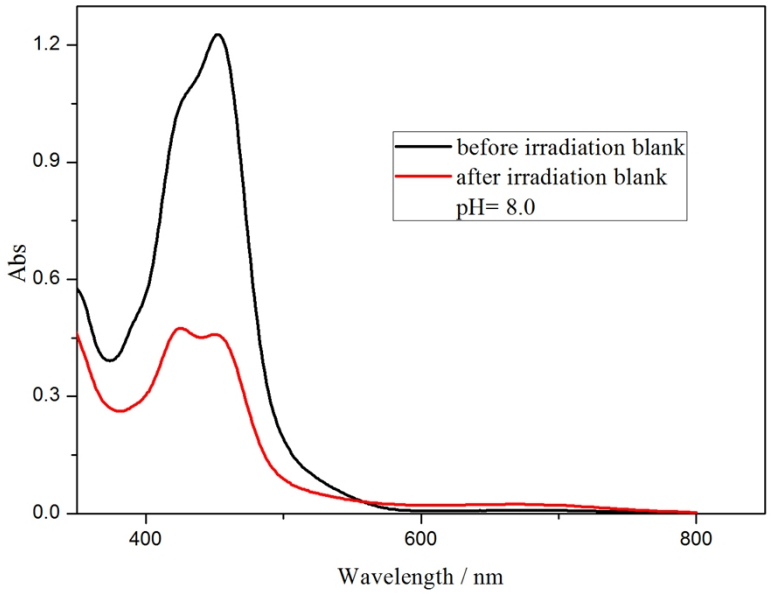

Figure S4.UV-vis spectral changes during the photocatalytic O_2 evolution without any catalyst. The black line shows the absorption of aqueous borate buffer solutions (pH = 8.0, 80 mM) containing $[Ru(bpy)_3](ClO_4)_2$ (1.0 mM) and $Na_2S_2O_8$ (5.0 mM). The red line shows the absorption of above solution after 9 min of irradiation. (the concentration of $[Ru(bpy)_3]^{2+}$ decreased by 62.7%)

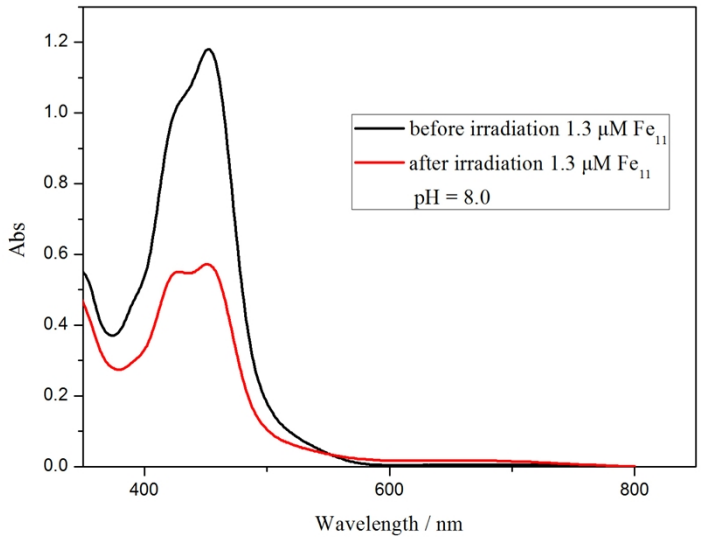

Figure S5. UV-vis spectral changes during the photocatalytic O_2 evolution with Fe_{11} POM. The black line shows the absorption of aqueous borate buffer solutions (pH = 8.0, 80 mM) containing $[Ru(bpy)_3](ClO_4)_2$ (1.0 mM) , $Na_2S_2O_8$ (5.0 mM) and and Fe_{11} POM (1.3 μM) . The red line shows the absorption of above solution after 9 min of irradiation. (the concentration of $[Ru(bpy)_3]^{2+}$ decreased by 51.5%)

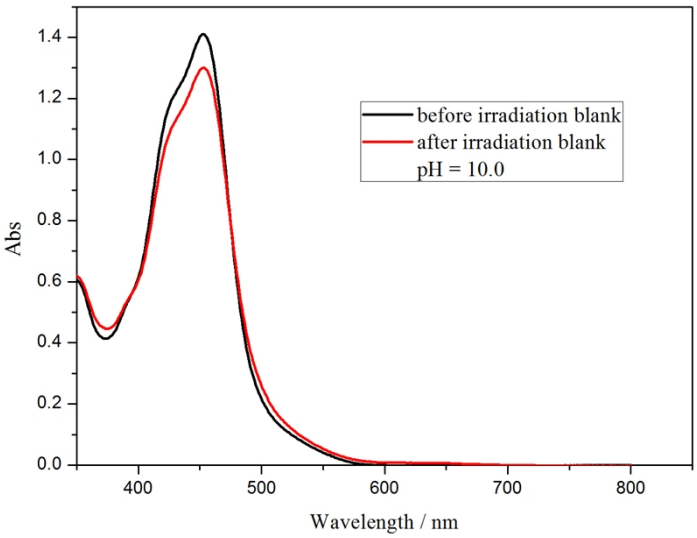

Figure S6.UV-vis spectral changes during the photocatalytic O_2 evolution without any catalyst. The black line shows the absorption of aqueous borate buffer solutions (pH = 10.0, 80 mM) containing $[Ru(bpy)_3](ClO_4)_2$ (1.0 mM) and $Na_2S_2O_8$ (5.0 mM). The red line shows the absorption of above solution after 9 min of irradiation. (the concentration of $[Ru(bpy)_3]^{2+}$ decreased by 7.8%)

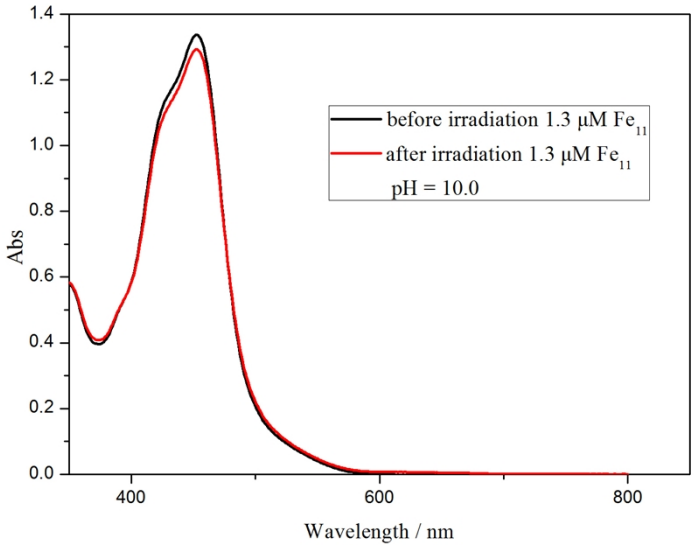

Figure S7. UV-vis spectral changes during the photocatalytic O_2 evolution with Fe_{11} POM .The black line shows the absorption of aqueous borate buffer solutions (pH = 10.0, 80 mM) containing $[Ru(bpy)_3](ClO_4)_2$ (1.0 mM), $Na_2S_2O_8$ (5.0 mM) and Fe_{11} POM (1.3 μM). The red line shows the absorption of above solution after 9 min of irradiation. (the concentration of $[Ru(bpy)_3]^{2+}$ decreased by 3.4%)

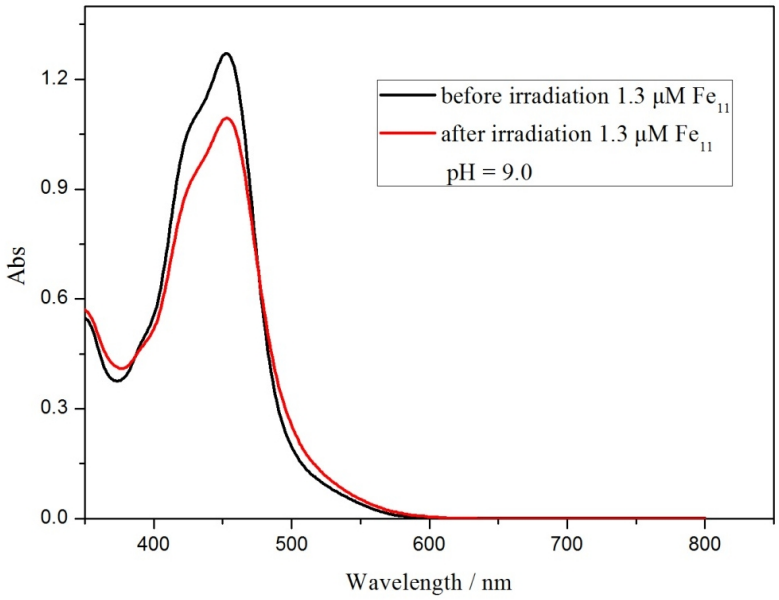

Figure S8. UV-vis spectral changes during the photocatalytic O_2 evolution with Fe_{11} POM. The black line shows the absorption of aqueous borate buffer solutions (pH = 9.0, 80 mM) containing $[Ru(bpy)_3](ClO_4)_2$ (1.0 mM) , $Na_2S_2O_8$ (5.0 mM) and and Fe_{11} POM (1.3 μM). The red line shows the absorption of above solution after 9 min of irradiation. (the concentration of $[Ru(bpy)_3]^{2+}$ decreased by 13.9%)

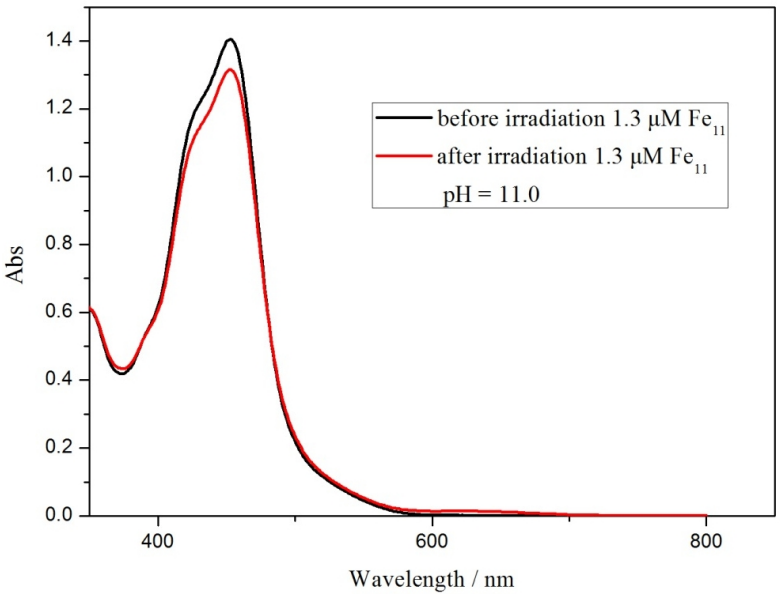

Figure S9. UV-vis spectral changes during the photocatalytic O_2 evolution with Fe_{11} POM. The black line shows the absorption of aqueous borate buffer solutions (pH = 11.0, 80 mM) containing $[Ru(bpy)_3](ClO_4)_2$ (1.0 mM) , $Na_2S_2O_8$ (5.0 mM) and and Fe_{11} POM (1.3 μM). The red line shows the absorption of above solution after 9 min of irradiation. (the concentration of $[Ru(bpy)_3]^{2+}$ decreased by 6.3%)

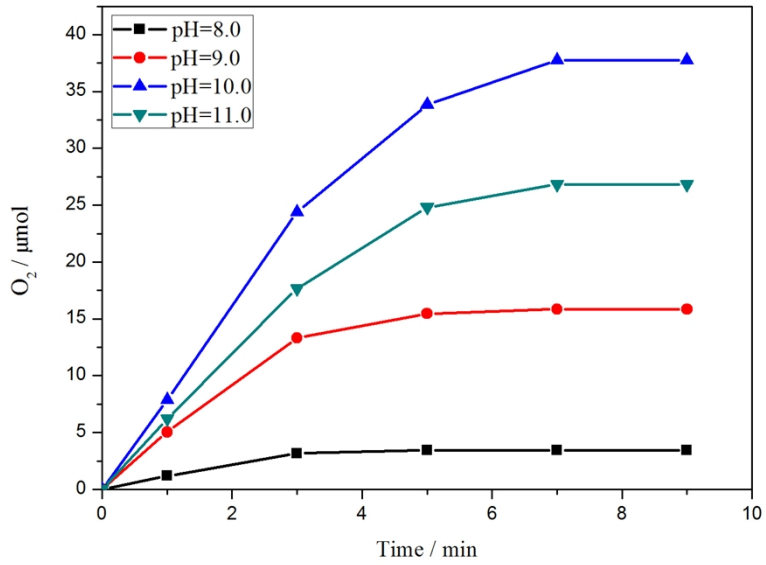

Figure S10. Kinetics of O_2 formation in the photocatalytic system under various pH conditions (pH = 8.0, 80 mM NaBi, black; pH = 9.0, 80 mM NaBi, red; pH = 10.0, 80 mM NaBi, blue; pH = 11.0, 80 mM NaBi, green). Conditions: LED lamp ($\lambda \geq 420$ nm), 1.3 μM **1**, 1.0 mM $[Ru(bpy)_3](ClO_4)_2$, 5.0 mM $Na_2S_2O_8$, total reaction volume is 16mL and overall volume is ~21mL, vigorous agitation using a magnetic stirrer.

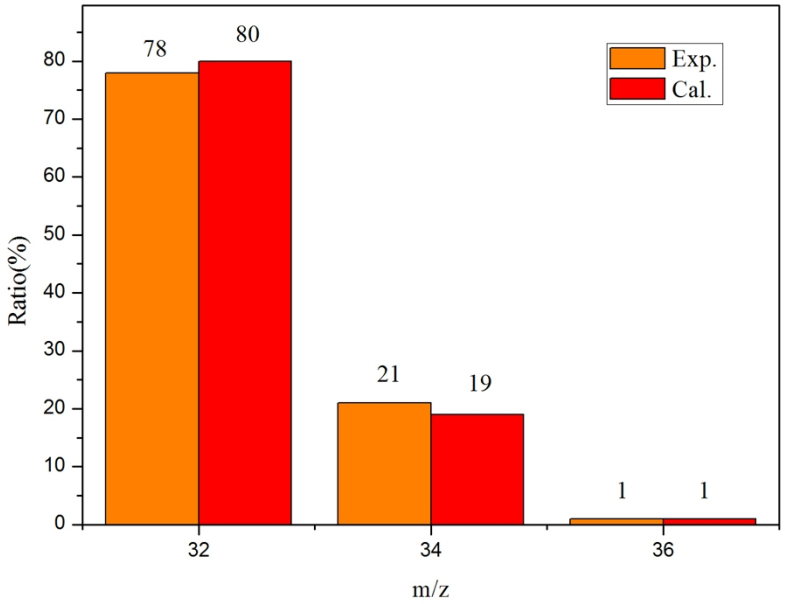

Figure S11. Observed and theoretical relative abundances of ^{18}O-labeled and unlabeled oxygen evolved during the photocatalytic oxidation of a buffer solution (4.5 mL) prepared with $H_2{}^{18}O$-enriched water (10.8% $H_2{}^{18}O$) containing **1** (1.3 μM) , $[Ru(bpy)_3]^{2+}$ (1.0 mM) and $Na_2S_2O_8$ (5.0 mM) (yellow, observed mass intensity; red, calculated values assuming that evolved O_2 results exclusively from water).

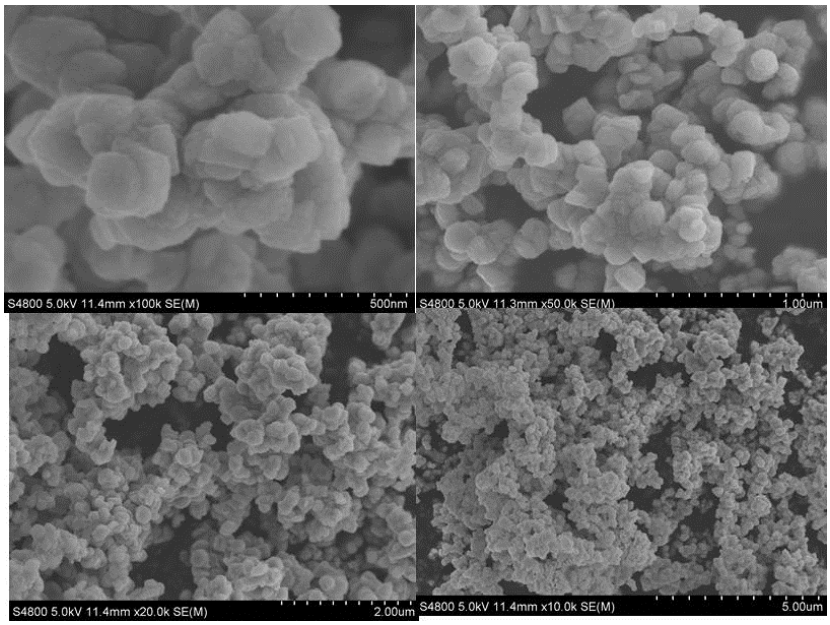

Figure S12. SEM images of commercially available Fe_2O_3 particles.

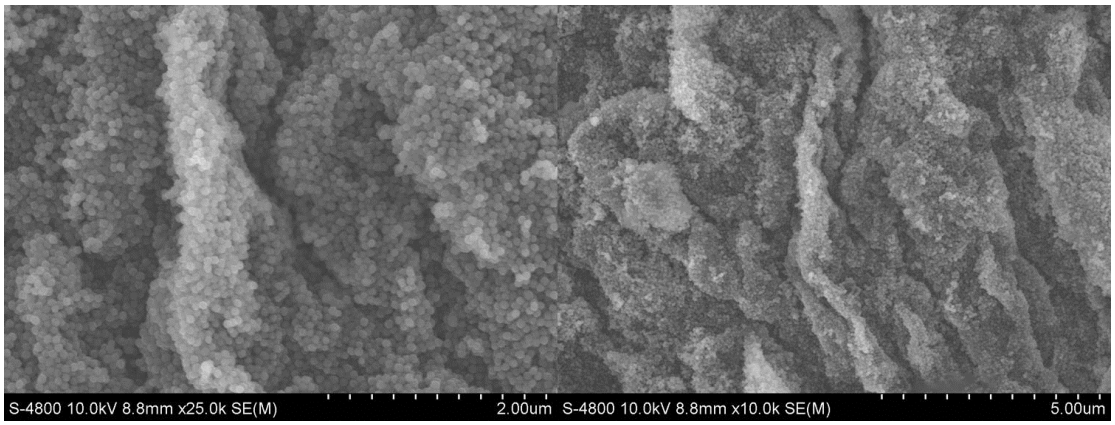

Figure S13. SEM images of α-Fe_2O_3 nanoparticles.

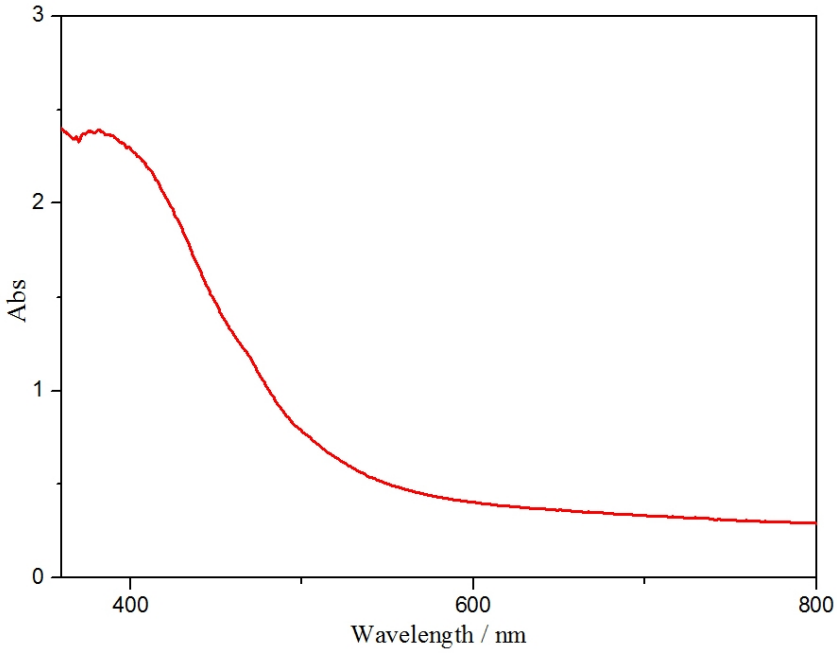

Figure S14. UV-Vis diffuse reflectance spectrum of **1**.

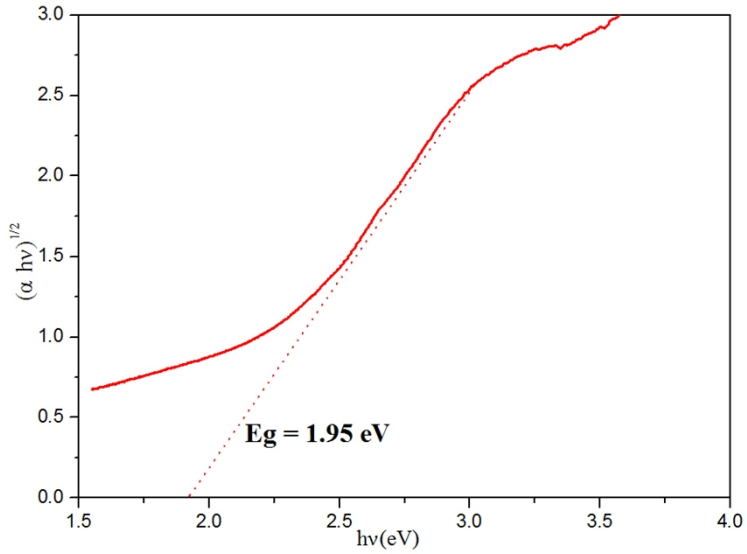

Figure S15. $(ahν)^{1/2}$ versus hν curve of **1**. The red dashed lines are the tangents of the curves. The intersection value is the band gap.

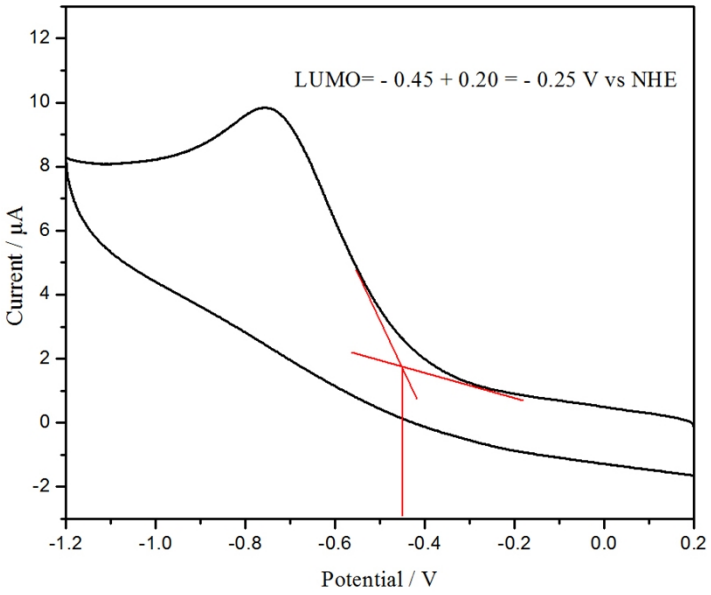

Figure S16. Cyclic voltammogram of 2.5×10^{-4} M **1** in pure water (pH = 7.0) at a scan rate of 100 mV/s. The working electrode was glassy carbon and the reference electrode was Ag/AgCl.

With Ag/AgCl electrode as reference electrode, relative to that NHE potential of 0.20 eV, the formula for calculating level:

E_{HOMO}= -(eE^{ox}+4.5 +0.20) eV = -(eE^{ox}+4.70) eV

E_{LUMO}= -(eE^{red}+4.5 +0.20) eV = -(eE^{red}+4.70) eV

$Eg=E_{HOMO}-E_{LUMO}$ E^{red}= -0.25 V

E_{LUMO}= -(Ee^{red}+4.5+0.20) eV = -(-0.25+4.70) eV = -4.45 eV Eg = 1.95 eV

E_{HOMO} = -(1.95+4.45) eV= -6.40 eV

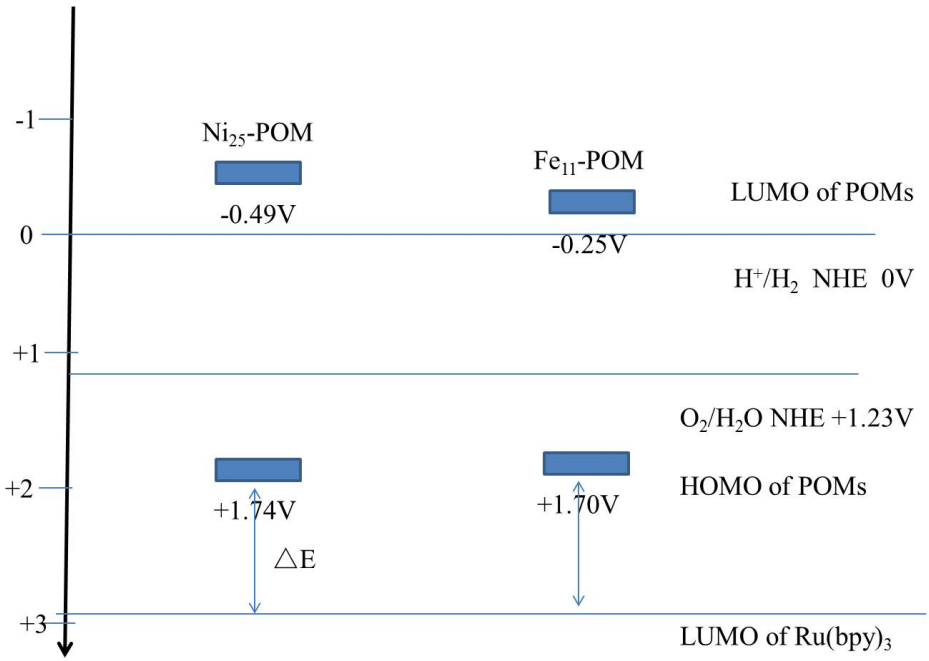

Figure S17. The band gap structures of Ni_{25}-POM and compounds **1**. ΔE = HOMO ($[Ru(bpy)_3]^{3+}$) – HOMO(POMs).

			Diam. (nm)	% Intensity	Width (nm)
Z-Average (d.nm):	0.000	Peak 1:	0.000	0.0	0.000
PdI:	0.000	Peak 2:	0.000	0.0	0.000
Intercept:	0.00	Peak 3:	0.000	0.0	0.000
Result quality	Refer to quality report				

Figure S18. Particle size distribution measured by DLS in a solution of **1** (1.30 μM), $[Ru(bpy)_3](ClO_4)_2$ (1.0 mM), $Na_2S_2O_8$ (5.0 mM) in 80 mM, pH = 10.0 borate buffer after 9 min of irradiation

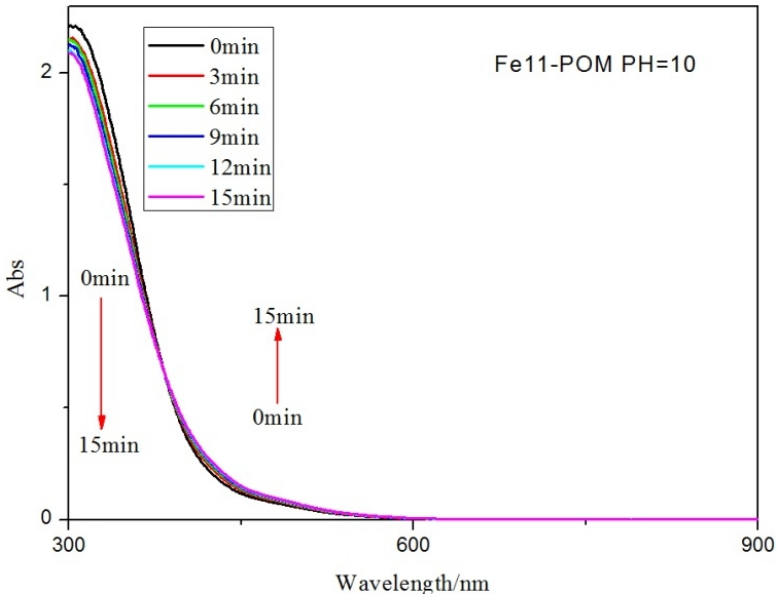

Figure S19. Time-dependent UV-vis absorption spectra of **1** (50 μM) over 15 min in borate buffer (80 mM, pH 10.0)

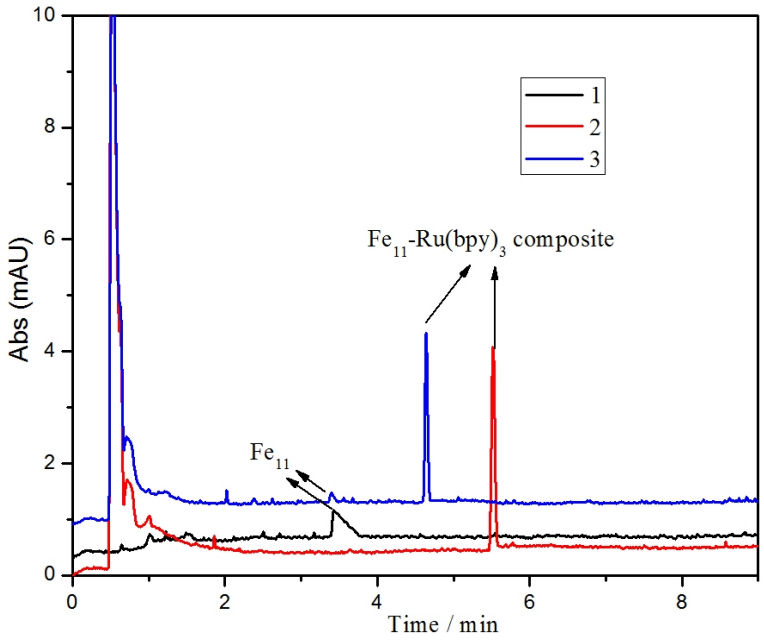

Figure S20. An electropherogram for 5.0 μM of compounds **1**. Black lines: 5 μM of compounds **1** in a 20 mM sodium borate buffer solution (pH = 10.0). Red lines: 5.0 μM of compounds **1** in a 20 mM sodium borate buffer solution (pH = 9.0) containing $[Ru(bpy)_3]^{2+}$ (1 mM), $Na_2S_2O_8$ (5 mM) before illumination. Blue lines: 5.0 μM of compounds **1** in a 20 mM sodium borate buffer solution (pH = 10.0) containing $[Ru(bpy)_3]^{2+}$ (1 mM), $Na_2S_2O_8$ (5 mM) after 9 min of irradiation. Experimental conditions for capillary electrophoresis: Fused-silica capillaries (50μm i.d., 365μm o.d., Hebei Yongnian Factory, China) with total length of 50.2 cm and effective length of 10 cm were used. The detection wavelength was set at 214 nm. The running buffer for CE separation was 20 mM sodium borate buffer (pH 10.0). The separation voltage was set at -20 kV. The sample was injected into the capillary (0.5psi, 3 s).

The peaks of compounds **1** was not observed before photocatalytic reactions, because formation of POM-$Ru(bpy)_3$ composite precipitates is more than that after photocatalytic reactions .

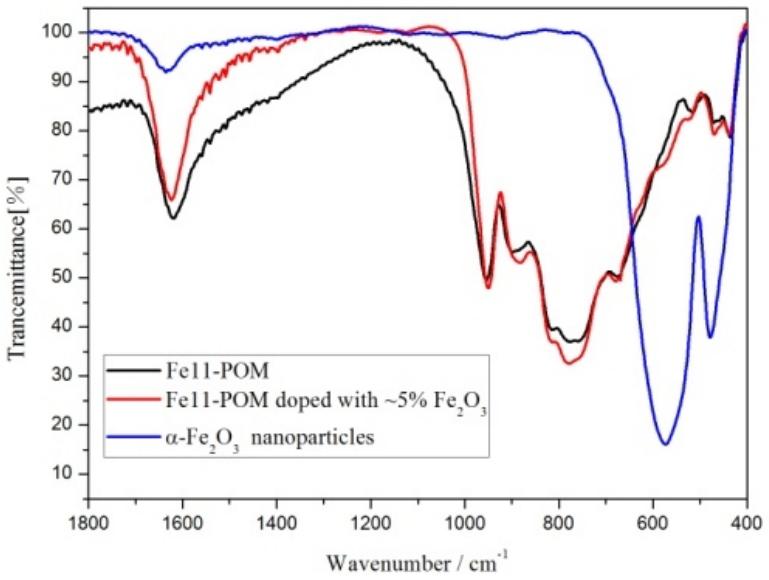

Figure S21. FT-IR spectra of **1** and α-Fe_2O_3 nanoparticles. Black: spectrum of **1**. Red: **1** doped with ~5% α-Fe_2O_3 nanoparticles. Blue: α-Fe_2O_3 nanoparticles, highlighting the characteristic peaks at 480 cm^{-1} and 580 cm^{-1} that would be visible if **1** decomposes to α-Fe_2O_3 nanoparticles under catalytic conditions.

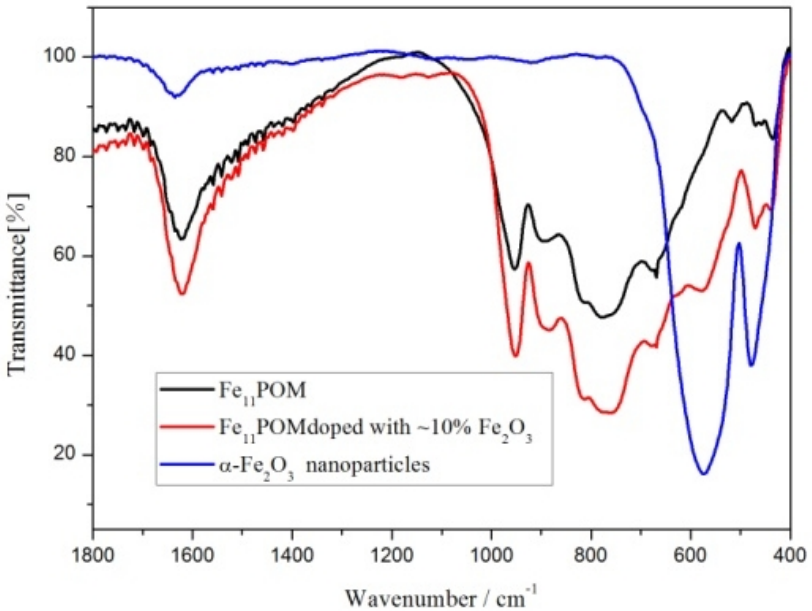

Figure S22. FT-IR spectra of **1** and α-Fe_2O_3 nanoparticles. Black: spectrum of **1**. Red: **1** doped with ~10% α-Fe_2O_3 nanoparticles. Blue: α-Fe_2O_3 nanoparticles, highlighting the characteristic peaks at 480 cm^{-1} and 580 cm^{-1} that would be visible if **1** decomposes to α-Fe_2O_3 nanoparticles under catalytic conditions.

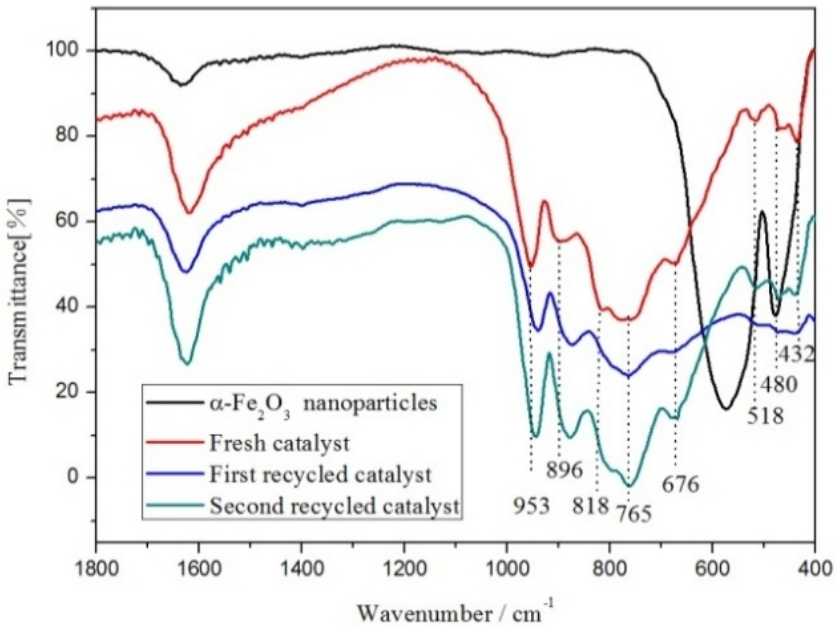

Figure S23. FT-IR spectra of **1**, recovered catalyst and α-Fe_2O_3 nanoparticles: fresh catalyst, red; first recycled catalyst, blue; second recycled catalyst, green; α-Fe_2O_3 nanoparticles, black.

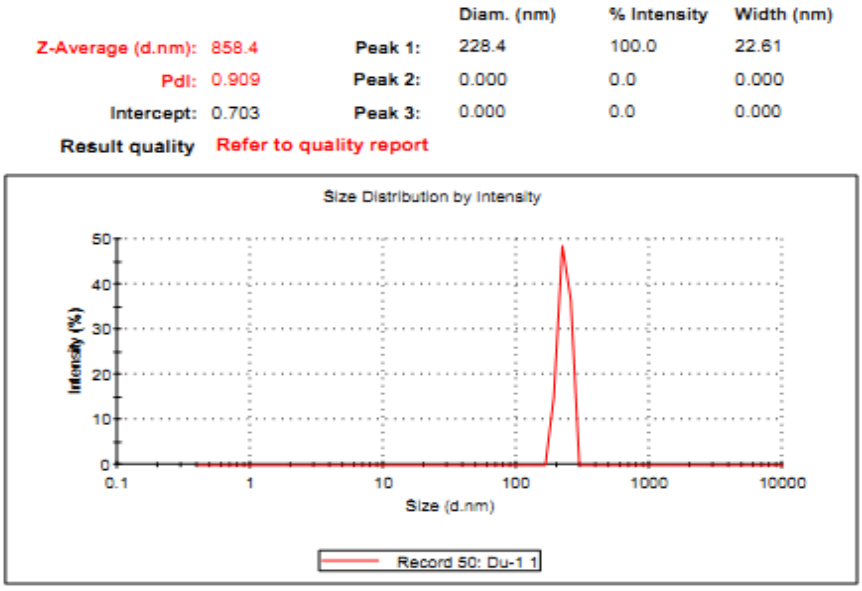

Figure S24. Particle size distribution measured by DLS in a solution of 99.0% of **1** and 1.0% $Fe(NO_3)_3$ (**1** + $Fe(NO_3)_2$ = 1.3 μM), $[Ru(bpy)_3](ClO_4)_2$ (1.0 mM), $Na_2S_2O_8$ (5.0 mM) in 80 mM borate buffer (pH = 10.0) after 9 min of irradiation.

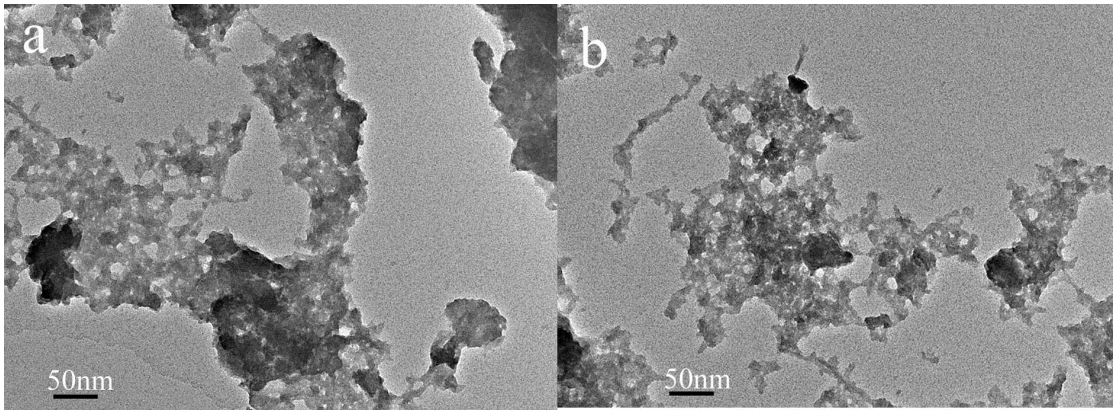

Figure S25.TEM images of the fresh catalyst (a) and recovered catalyst (b).

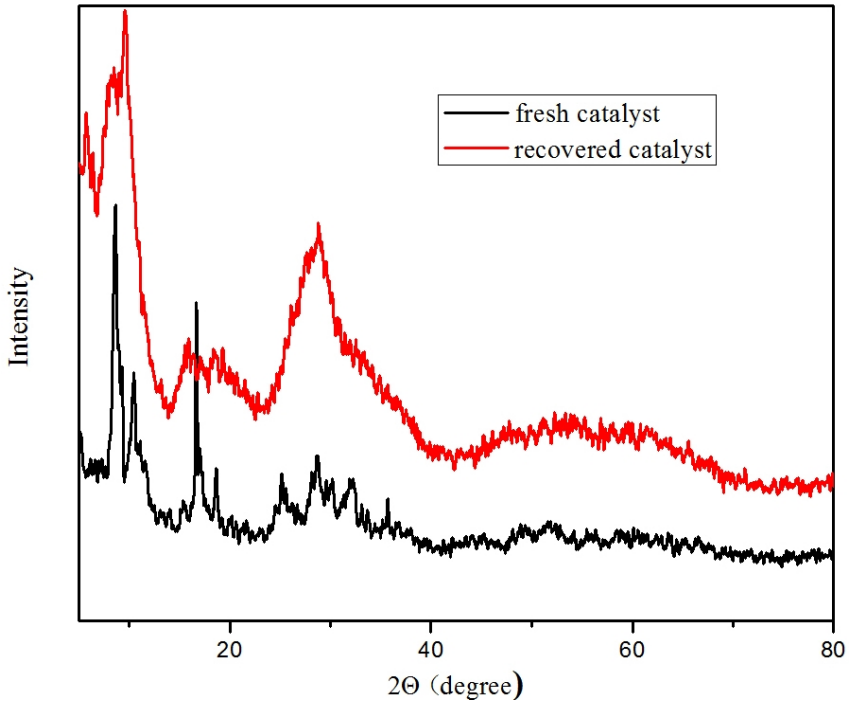

Figure S26. XRD of fresh catalyst (black) and recovered catalyst (red).

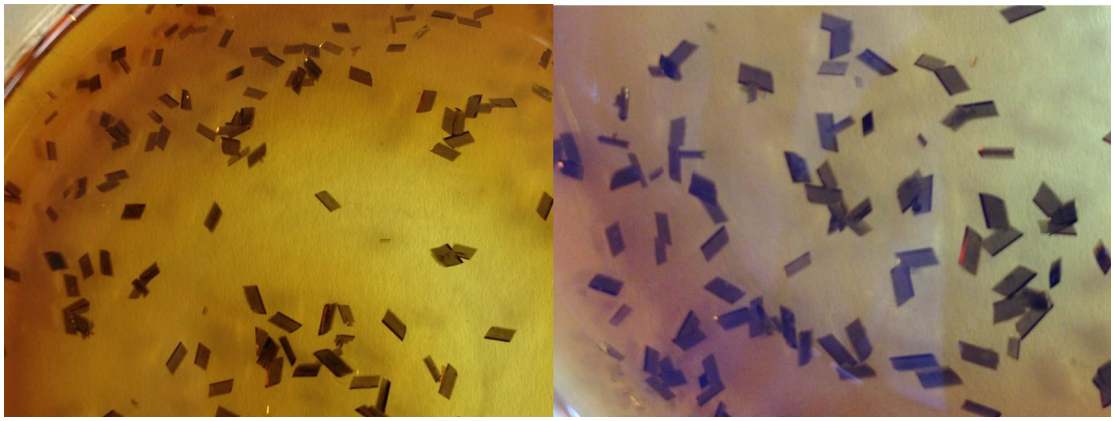

Figure S27. Images for crystal of **1**.

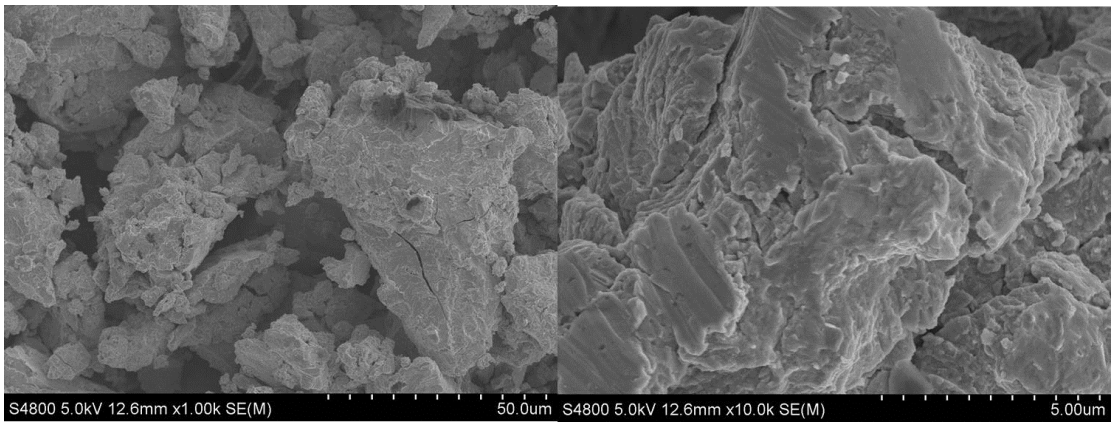

Figure S28.SEM images of **1**

References

1. X. Du, J. Zhao , J. Mi , Y. Ding , P. Zhou, B. Ma, J. Zhao and J. Song, *Nano Energy*, 2015, **DOI:10.1016/j.nanoen.2015.06.025.**
2. T. Raming, A. Winnubst, C. M. van Kats and A. Philipse, *J. Colloid Interface Sci.*, 2002, **249**, 346-350.
3. U. Kortz, M. G. Savelieff, B. S. Bassil, B. Keita and L. Nadjo, *Inorg. Chem.*, 2002, **41**, 783-789.
4. F. Zonnevijlle, C. M. Tourne and G. F. Tourne, *Inorg. Chem.*, 1982, **21**, 2751-2757.

5. Z. Huang, Z. Luo, Y. V. Geletii, J. W. Vickers, Q. Yin, D. Wu, Y. Hou, Y. Ding, J. Song, D. G. Musaev, C. L. Hill and T. Lian, *J. Am. Chem. Soc.*, 2011, **133**, 2068-2071.
6. G. Zhu, Y. V. Geletii, P. Kogerler, H. Schilder, J. Song, S. Lense, C. Zhao, K. I. Hardcastle, D. G. Musaev and C. L. Hill, *Dalton Trans.*, 2012, **41**, 2084-2090.
7. S. Tanaka, M. Annaka and K. Sakai, *Chem. Commun.*, 2012, **48**, 1653-1655.
8. C. Leung, S. Ng, C. Ko, W. Man, J. Wu, L. Chen and T. Lau, *Energy Environ. Sci.*, 2012, **5**, 7903-7907.
9. D. Hong, J. Jung, J. Park, Y. Yamada, T. Suenobu, Y.-M. Lee, W. Nam and S. Fukuzumi, *Energy Environ. Sci.*, 2012, **5**, 7606-7616.
10. N. S. McCool, D. M. Robinson, J. E. Sheats and G. C. Dismukes, *J. Am. Chem. Soc.*, 2011, **133**, 11446-11449.
11. G. Zhu, E. N. Glass, C. Zhao, H. Lv, J. W. Vickers, I. Geletii, D. G. Musaev, J. Song and C. L. Hill, *Dalton Trans.*, 2012, **41**, 13043-13049.
12. C. Besson, Z. Huang, Y. V. Geletii, S. Lense, K. I. Hardcastle, D. G. Musaev, T. Lian, A. Proust and C. L. Hill, *Chem. Commun.*, 2010, **46**, 2784-2786.
13. P. Car, M. Guttentag, K. K. Baldridge, R. Alberto and G. R. Patzke, *Green Chem.*, 2012, **14**, 1680-1688.
14. L. Tong, Y. Wang, L. Duan, Y. Xu, X. Cheng, A. Fischer, M. r. S. Ahlquist and L. Sun, *Inorg. Chem.*, 2012, **51**, 3388-3398.
15. G. Chen, L. Chen, S. Ng, W. Man and T. Lau, *Angew.Chem., Int. Ed.*, 2013, **52**, 1789-1791.
16. D. Hong, S. Mandal, Y. Yamada, Y. M. Lee, W. Nam, A. Llobet and S. Fukuzumi, *Inorg. Chem.*, 2013, **52**, 9522-9531.
17. F. Evangelisti, R. Guttinger, R. More, S. Luber and G. R. Patzke, *J.Am.Chem.Soc.*, 2013, **135**, 18734-18737.
18. F. Evangelisti, P. Car, O. Blacque and G. R. Patzke, *Catal.Sci.Technol.*, 2013, **3**, 3117.
19. G. Chen, L. Chen, S. M. Ng and T. C. Lau, *ChemSusChem*, 2014, **7**, 127-134.
20. X. B. Han, Z. M. Zhang, T. Zhang, Y. G. Li, W. Lin, W. You, Z. M. Su and E. B. Wang, *J. Am. Chem. Soc.*, 2014, **136**, 5359-5366.
21. H. Lv, J. Song, Y. V. Geletii, J. W. Vickers, J. M. Sumliner, D. G. Musaev, P. Kogerler, P. F. Zhuk, J. Bacsa, G. Zhu and C. L. Hill, *J. Am. Chem. Soc.*, 2014, **136**, 9268-9271.
22. R. Xiang, Y. Ding and J. Zhao, *Chem. Asian. J.*, 2014, **9**, 3228-3237.
23. X. B. Han, Y. G. Li, Z. M. Zhang, H. Q. Tan, Y. Lu and E. B. Wang, *J. Am. Chem. Soc.*, 2015, **137**, 5486-5493.
24. W. C. Ellis, N. D. McDaniel, S. Bernhard and T. J. Collins, *J. Am. Chem. Soc.*, 2010, **132**, 10990-10991.
25. J. L. Fillol, Z. Codolà, I. Garcia-Bosch, L. Gómez, J. J. Pla and M. Costas, *Nat. Chem.*, 2011, **3**, 807-813.